THESIS FOR THE DEGREE OF DOCTOR OF PHILOSOPHY
IN
THERMO AND FLUID DYNAMICS

Turbulence-resolving Simulations of Swirling Flows

by

ARDALAN JAVADI

Department of Applied Mechanics
Division of Fluid Dynamics
CHALMERS UNIVERSITY OF TECHNOLOGY
Gothenburg, Sweden 2016

Turbulence-resolving Simulations of Swirling Flows
ARDALAN JAVADI
ISBN 978-91-7597-362-3

Doktorsavhandlingar vid Chalmers tekniska högskola
Ny serie nr. 4043
ISSN 0346-718X

Department of Applied Mechanics
Division of Fluid Dynamics
Chalmers University of Technology
SE-412 96 Gothenburg
Sweden
Telephone: +46 (0)31-772 1000

Cover:
Iso-surface of q-criterion colored by pressure in the U9 Kaplan turbine using DDES-SA, left) best-efficiency point, right) part-load.

This document was typeset using LaTeX

Printed at Chalmers Reproservice
Gothenburg, Sweden 2016

Turbulence-resolving Simulations of Swirling Flows

Ardalan Javadi

Department of Applied Mechanics
Division of Fluid Dynamics
Chalmers University of Technology

Abstract

A series of numerical investigations is undertaken using a wide range of turbulence models including conventional and non-conventional URANS models, hybrid URANS-LES methods and LES to capture a large variety of physical mechanisms that produce pressure pulsations in the swirling flows. The available knowledge about these pulsations, which are usual in hydropower, are still far from complete. When the swirl is moderately low, a stable on-axis structure generates in the pipe. If the swirl exceeds a certain level, the flow patterns associated with the swirl dominated vortex motions vacillate. A key feature of strongly swirling flows is vortex breakdown. The vortex breakdown is an abrupt change in the core of a slender vortex and typically develops downstream into a recirculatory "bubble" or a helical pattern. The swirl effects are usually seen as either the desired result of design or unavoidable, possibly unforeseen, side effects which comprise a forced vortex core centered around its axis of rotation. The vortex breakdown is an inviscid process and the pulsations caused by the vortex breakdown and their impact on the efficiency and hydraulic structures of water turbines depend on the flow rate, the velocity distribution after the runner, the shape of the draft tube, and the dynamic response of the whole hydraulic structure. The high level of unsteadiness in the flow field necessitates the utilization of appropriate turbulence treatments to predict the complexity of the flow structures.

Time-accurate Reynolds-averaged Navier-Stokes (URANS) models are primarily useful for capturing large-scale flow structures, while the details of the small-scale turbulence eddies are filtered out in the averaging process. In many cases also the large-scale structures are damped by the URANS modeling which is formulated to model all the turbulence. The swirling flows in a pipe are dominated by large-scale detached eddies, therefore the URANS models should be capable of predicting the flow fields. The quality of the URANS results is very dependent on the underlying turbulence model. The knowledge about URANS is limited to the simplest (most robust) linear eddy-viscosity models which are available in the proprietary codes. The inability of the conventional linear eddy-viscosity models available in a CFD code should thus not be generalized to the URANS method alone. The conventional linear eddy-viscosity model provides a direct link between the turbulent stress tensor and the mean strain rate, forcing them to be directly in phase, which is wrong. In the highly swirling flows, the curvature of the streamlines should be taken into account for a better predicting of the flow fields. Reynolds Stress Models (RSM) have the potential to significantly improve the flow predictions by resolving anisotropy and incorporating more sensitivity and receptivity of the underlying instabilities and unsteadiness. Since they are difficult to use they are

not widely used in industry. Most of the RSMs are not robust for highly swirling flows because of instability in the rapid part of the pressure-strain term in the transport equation. The Explicit Algebraic Reynolds Stress Models (EARSMs) are simplified RSMs that are much more numerically and computationally robust and have been found to be comparable to standard two-equation models in computational effort. The EARSMs assume that the Reynolds stress tensor can be expressed in the strain and vorticity rate tensors.

A more advanced approach, also called the second generation URANS method, is the hybrid URANS-LES method which is capable of capturing the high level of unsteadiness and handling the anisotropic and highly dynamic character of turbulent swirling flows. An extended series of turbulence models is scrutinized in this work while the main focus is on the Detached-eddy simulation (DES) method. The DES method is a promising hybrid URANS-LES strategy capable of simulating internal flows dominated by large-scale detached eddies at practical Reynolds numbers. Another hybrid URANS-LES method is scale-adaptive simulation (SAS). This method is based on detecting the unsteadiness according to the velocity gradients in the flow field. This method gives better results than LES in a highly swirling flow in a pipe using a relatively coarse resolution.

Keywords: Hydropower, Swirling Flow, Vortex Breakdown, Flow Control, Turbulence Modeling, URANS, Hybrid URANS-LES, DDES, SAS, LES

To my parents
Sara and Ali

Acknowledgements

The research presented was carried out as a part of the "Swedish Hydropower Center - SVC". SVC is established by the Swedish Energy Agency, EnergiForsk and Svenska Kraftnät together with Luleå University of Technology, The Royal Institute of Technology, Chalmers University of Technology and Uppsala University, www.svc.nu. The computational facilities are provided by C^{3}SE, the center for scientific and technical computing at Chalmers University of Technology, and SNIC, the Swedish National Infrastructure for Computing.

I acknowledge the supports of Håkan Nilsson. This thesis might not has been written with this quality without his endorsing.

Preface

This thesis consists of three chapters and two appendices. Introduction identifies the physical mechanisms involved in the swirling flows and presents an overview of the appropriate numerical methods. Summary of papers explains the methodology and outcomes of the papers and finally Conclusion delineates the main products of the thesis. This thesis also consists of two appendices. Appendix A is about the implementation of two turbulence models, the elliptic-blending Reynolds stress model (EBRSM), and implementation of a hybrid URANS-LES method coupled with EBRSM. Appendix B includes eight papers, which are the main scientific contribution of the work.

List of publications

This thesis consists of the following publications:

Paper A A. Javadi and H. Nilsson. "LES and DES of swirling flow with rotor-stator interaction". *Progress in Hybrid RANS-LES Modelling*. Ed. by S. Girimaji. Vol. 130. Springer-Verlag, 2014, pp. 457–468

Paper B A. Javadi and H. Nilsson. "A comparative study of scale adaptive and large-eddy simulations of highly swirling turbulent flow through an abrupt expansion". *IOP Conf. Ser.: Earth Environ. Sci.* Vol. 22. 2. 022017. 2014

Paper C A. Javadi and H. Nilsson. LES and DES of strongly swirling turbulent flow through a suddenly expanding circular pipe. *Comput. Fluids* **107** (2015), pp. 301–313. DOI: 10.1016/j.compfluid.2014.11.014

Paper D A. Javadi and H. Nilsson. Time-accurate numerical simulations of swirling flow with rotor-stator interaction. *Flow Turbul. Combust.* **95** (2015), pp. 755–774. DOI: 10.1007/s10494-015-9632-2

Paper E A. Javadi, E. Krane, and H. Nilsson. "Exploration of rotation/curvature correction method in hydropower application". *Turbulence, Heat and Mass Transfer 8*. Bosnia and Herzegovina, Sarajevo, 2015

Paper F A. Javadi, A. Bosioc, H. Nilsson, S. Muntean, and R. Susan-Resiga. Experimental and numerical investigation of the precessing helical vortex in a conical diffuser, with rotor-stator interaction. *ASME J. Fluids Eng.* (2016). DOI: 10.1115/1.4033416

Paper G A. Javadi and H. Nilsson. Detailed numerical simulations of a Kaplan turbine with rotor-stator interaction using turbulence-resolving simulations (2016). submitted to a scientific journal

Paper H A. Javadi and H. Nilsson. Active flow control of the vortex rope in a swirl generator. *Will be Published in Eng. App. Comput. Fluid Dyn.* (2016)

Division of work

Paper A-C
Ardalan Javadi did all the work on geometry cleaning, mesh generation, numerical simulations, analysis, and writing of the paper. Håkan Nilsson gave feedback in the writing of the paper.

Paper D
Ardalan Javadi implemented and verified the delayed DES SST $k-\omega$ turbulence model, did the pre-processing, processing and post-processing of the numerical simulations and writing of the paper. Håkan Nilsson gave feedback in the writing of the paper.

Paper E
Ardalan Javadi implemented the SST $k-\omega$ turbulence model with curvature correction modeling, verified the model by simulating the flow in a swirl generator and wrote the paper. Ardalan Javadi and Håkan Nilsson supervised the master thesis work of Erik Krane.

Paper F
Ardalan Javadi did all the work on geometry cleaning, mesh generation, numerical simulations, analysis, and writing of the paper. Alin Bosioc did experimental measurements and wrote the sections related to it. Håkan Nilsson, Sebastian Muntean and Romeo Susan-Resiga gave feedback in the writing of the paper.

Paper G
Ardalan Javadi implemented and verified the explicit algebraic Reynolds stress model coupled with $k-\omega$ baseline, did the pre-processing, processing and post-processing of the numerical simulations and writing of the paper. Håkan Nilsson gave feedback in the writing of the paper.

Paper H
Ardalan Javadi prepared the idea of the flow control method and did all the work on geometry cleaning, mesh generation, numerical simulations, analysis, and writing of the paper.

Other relevant publications

Other publications related to thesis:

Publication I A. Javadi and H. Nilsson. "Advanced numerical prediction of strongly swirling turbulent flows". *5th International Workshop on Cavitation and Dynamic Problems in Hydraulic Machinery, September 9-11, Lausanne, Switzerland*. Vol. 23. 2013

Publication II A. Javadi and H. Nilsson. "Unsteady numerical simulation of the flow in the U9 Kaplan turbine model". *IOP Conf. Ser.: Earth Environ. Sci.* Vol. 22. 2. 022001. 2014

Publication III A. Javadi, A. Bosioc, H. Nilsson, S. Muntean, and R. Susan-Resiga. "Velocity and pressure fluctuations induced by the precessing helical vortex in a conical diffuser". *IOP Conf. Ser.: Earth Environ. Sci.* Vol. 22. 3. 032009. 2014

Publication IV A. Javadi and H. Nilsson. "Active flow control of vortex rope in a conical diffuser". *IAHR WG Meeting on Cavitation and Dynamic Problems in Hydraulic Machinery and Systems, Ljubljana*. 2015

Publication V A. Javadi, A. Bosioc, H. Nilsson, S. Muntean, and R. Susan-Resiga. *Swirling flow in a conical diffuser generated with rotor-stator interaction*. Ed. by W. Rodi. 2016. URL: `http://qnet-ercoftac.cfms.org.uk/w/index.php/Main_Page`

Contents

1 Introduction

Confined turbulent swirling flows are encountered in many industrial applications, such as hydraulic turbines, gas turbine combustors and internal combustion engines. A key feature of the strongly swirling flows is vortex breakdown. Vortex breakdown is an abrupt change in the core of a slender vortex and typically develops downstream into a recirculatory "bubble" or a helical pattern [13, 14]. The vortex breakdown may be beneficial, e.g. increasing heat transfer or the combustion rate in heat exchangers and combustors, or detrimental, e.g. yielding pressure pulsations in hydraulic turbines. The characteristics of various breakdown states (or modes) in swirling flows depend mainly on the swirl number (Sr),

$$Sr = \frac{\int_0^R U_\theta U_a r^2 dr}{R\int_0^R U_a^2 r dr}, \tag{1.1}$$

where U_a is the axial velocity, U_θ is the tangential velocity and R is the cross-section radius.

Gupta et al. [16] observed that the vortex breakdown for turbulent flows at low swirl numbers is dominated by large-scale unsteadiness due to the onset of a slowly precessing helical vortex core. The precessing vortex core is related to the oscillatory motion of non-turbulent coherent structures, yielding the dominant frequency of the energy spectrum. It is known that, as the swirl number increases, the oscillatory motion of the coherent structure becomes more pronounced [17]. For nonswirl flow, the jet can rotate in either direction, while when a slight swirl is included, the precessing vortex counter-rotates to the direction of the swirl [18]. Several modes of precession are observed as the swirl intensity increases, in which the precession, as well as the spiral structure, reverses direction [19]. The inclusion of a slight swirl ($Sr = 0.1$) at the inlet can reduce the helical precession speed and may cause the rotation of the precessing helical vortex to be against the mean swirl [18]. When the swirl increases to $Sr = 0.5$, a central recirculation zone occurs, which is a typical manifestation of vortex breakdown [18]. This central reversed flow is the result of a low-pressure region created by the centrifugal force. For swirling flow in a straight circular pipe at a fixed Reynolds number (Re), it is well known that, above a threshold swirl number, a disturbance develops along the vortex core, characterized by the onset of a limited region of reversed flow along the axis. This marks the transition from a supercritical to a subcritical swirling flow state [20]. As the swirl number increases to moderate levels, the flow is known to become more axisymmetric with an on-axis recirculation, marking the onset of bubble-type vortex breakdown.

The first analysis of sudden-expansion pipe flows was made by Borda [15] and the literature has since been concerned with confirming his expression for the overall loss. However, this flow is still not well understood, especially for strongly swirling flow, where the swirl number is about unity. There are only a handful detailed numerical studies that treat the coherent structures and vortex breakdown [2, 3]. At elevated swirl intensities ($Sr > 0.6$), the swirling jet emanating from the expansion is deflected toward the wall, the secondary recirculation region close to the corner contracts and reversal of the flow becomes evident near the centerline of the expansion [21]. The global frequency of the flow field belongs to the precessing helical vortex, which oscillates about the centerline

basically in a symmetrical fashion in spite of instantaneous asymmetries. The vortex core precession has been experimentally [21] and numerically [2, 3] observed to be both co-rotating and counter-rotating with the mean swirl direction. Dellenback et al. [21] reported that the precessing vortex core vanishes for $Sr \sim 0.4$, that there is a bubble-type vortex breakdown for $Sr < 0.6$ and that there is a strong on-axis tube of recirculating flow for higher swirl numbers. Thus, there is a maximum swirl number beyond which no precessing vortex core will occur. Dellenback et al. [21] also reported that the precession frequencies appear independent at large Reynolds numbers ($Re > 10^5$) but follow a slowly decreasing function of Re at lower Reynolds numbers.

The boundary conditions also play a prominent role to reproduce the physical mechanism of the vortex breakdown. The swirl intensity determines the occurrence of the vortex breakdown. The swirl depends on the axial and tangential velocity components that specify the physical mechanism of the breakdown. For swirling flows in a pipe, the former determines the radius of the vortex core and the later specifies the character of the on-axis axial velocity (jet- or wake-like). The inlet boundary condition is usually unknown at the draft tube inlet of the hydraulic turbomachines. To prevail this problem, the rotor-stator interaction which is the interaction between the guide vane and the runner blades, is considered and to retain the upstream effects on the flow in the draft tube.

The fixed-speed turbines in the power plants work most efficiently at the design point that delineates the best combination of the speed, head and discharge. At the design point (BEP), water turbines generally operate with little swirl entering the draft tube and without flow separations from the draft tube walls, whereas at off-design, at both full (HL) and part (PL) load, the flow leaving the turbine has a large tangential component. The hydraulic efficiency drops sharply due to this tangential component. It is known that a mitigated level of residual swirl downstream the runner delays boundary layer separation at the draft tube wall in the conical section and thus aids the pressure recovery [22]. The large swirl intensities, however, can decrease the performance by forming an on-axis recirculation regions [6, 7, 23]. Clausen et al. [22] showed that there is a narrow range of swirl intensities that prevents both recirculation and separation. When swirl increases, a vortex breakdown occurs.

The double-regulated Kaplan turbine stays close to the BEP efficiency by an adjustment of both the guide vane and runner blade angles with the flow rate. The key advantage of the axial-flow Kaplan turbine is the ability to operate at above 90% efficiency at low heads and high rotational speeds. The available range of runner blade angle adjustment is usually selected in a way as to permit high efficiency and a controlled residual swirl in the foreseen load range. Although the Kaplan turbine has a wide range of operation it may still have a significant residual swirl at PL. At PL, the range of flow where the draft tube swirl is organized to a vortex rope with a well-defined frequency is between 75 and 88% of Q_{BEP} [23]. Compared to Francis turbines, this range is much narrower and closer to the best-efficiency condition [23].

As mentioned above, the on-axis recirculation region and the ensuing helical vortex rope in the draft tube is a major source of loss. A prevention or mitigation of the vortex breakdown can significantly improve the stability of the flow and decrease the level of unsteadiness in the draft tube. Nishi et al. [24] used fins to mitigate the pulsation in the

draft tube. They showed that an installation of fins on the draft tube wall increases the operating range of a Francis turbine. Kjeldsen et al. [25] proposed a method to reduce the pressure pulsations in a Francis draft tube by injecting high speed water jets from distributed positions from the draft tube walls. The jets were injected tangentially and angled downstream with respect to the machine axis. The water consumption is however very high in that method, which reduces the efficiency of the machine. Recently the injection of a continuous jet from the runner crown center was studied by Susan-Resiga et al. [26], and Tănasă et al. [27]. The purpose was to mitigate the vortex rope by flushing it downstream with the jet. This leads to a significant reduction of the pressure pulsations of the vortex rope, but still at the cost of a high flow rate in the jet. A successful approach to prevent or mitigate the vortex breakdown should address the momentum deficit near the axis but not close to the wall.

A prevention or mitigation of the vortex breakdown can significantly improve the stability of the flow and decrease the level of unsteadiness in the draft tube. A successful approach should address the momentum deficit near the axis but not close to the wall. In this thesis, continuous slot jets with different axial and circumferential momentum fluxes are utilized to control the vortex breakdown and the vortex rope. The purpose is to use a small flow rate to manipulate the boundary layer at the crown to avoid the initiation of the vortex rope in the first place. The vortex breakdown control is an issue that should be genuinely addressed in future works.

Time-accurate Reynolds-averaged Navier-Stokes (URANS) models are primarily useful for capturing large-scale flow structures, while the details of the small-scale turbulence eddies are filtered out in the averaging process. In many cases also the large-scale structures are damped by the URANS modeling, which is formulated to model all the turbulence. The highly swirling flows are turbulent, unsteady-periodic and anisotropic. The URANS method is capable of predicting the large-scale structures in unsteady-periodic flows [28, 29]. Another approach to capture the high level of unsteadiness and to handle the anisotropic and highly dynamic character of turbulent swirling flows is the hybrid URANS-LES method. The partially averaging Navier-Stocks (PANS) method [31] uses a concept which corresponds to a filtering operation for a portion of the fluctuating scales. PITM [32] which is acronym for Partially Integrated Transport Model, is a seamless hybrid URANS-LES method. The amount of resolved energy is to be controlled by making the equations of the model dependent on the filter width. This can be achieved by using a transport equation for the dissipation rate that is a modification of the usual equation used in URANS. Scale-adaptive simulation (SAS) [30] is another hybrid URANS-LES method which is based on detecting the unsteadiness according to the velocity gradients in the flow field. An extended series of turbulence models is scrutinized in this work while the main focus is on the Detached-eddy simulation (DES) method [33]. DES is a promising hybrid URANS-LES strategy capable of simulating internal flows dominated by large-scale detached eddies at practical Reynolds numbers. The method aims at entrusting the boundary layers with URANS while the detached eddies in separated regions or outside the boundary layers are resolved using LES. DES predictions of massively separated flows, for which the technique was originally designed, are typically superior to those achieved using the URANS models, especially in terms of the three-dimensional and time-dependent features of the flow. The present work gives a thorough comparison

between the different levels of unsteady turbulence modeling, applied to swirling flow.

This thesis consists of advanced numerical simulations of the highly swirling flows through a sudden-expansion at practical Reynolds numbers. The capability of advanced numerical techniques is practiced in capturing the physical mechanisms engendered by the swirl. A swirl generator that generates highly swirling flows is studied with rotor-stator interaction using a wide range of turbulence treatments. The ability of the conventional eddy-viscosity models, the DDES method and LES turbulence models are scrutinized to predict the vortex breakdown in the conical diffuser. The experience gained with the investigation of the swirl generator is used to study the U9 Kaplan turbine model in different operating conditions. The conventional and non-conventional URANS models, and the DDES method is scrutinized using the rotor-stator interaction.

2 Summary of papers

2.1 Paper A

Paper A provides advanced numerical simulations of the flow in a swirl generator. A highly swirling turbulent flow engendered by the rotor-stator interaction of a swirl generator is investigated using LES and DES. A deeper understanding of such a flow physics is only possible with advanced numerical simulations which are rarely available in the literature. The delayed DES Spalart-Allmaras (DDES-SA), improved DDES-SA, shear stress transport DDES (DDES-SST), and a dynamic k-equation LES are studied. A mesh sensitivity study is performed on the hybrid methods, including the ability of capturing the details of the flow field. It is shown that all methods are capable of predicting the large-scale flow features, e.g. the vortex breakdown and the corresponding on-axis recirculation region. It is also shown that all hybrid methods capture most of the small-scale coherent structures, even with a relatively coarse mesh resolution. The various shielding functions of the hybrid methods are analyzed, distinguishing the location of the transition between URANS and LES mode. The high Reynolds number of the flow causes problems for LES to capture detailed unsteadiness of the flow, although the main feature of the flow (precessing vortex and vortex breakdown) is predicted reasonably. The precessing vortex occurs far from the wall. It is thus possible to use a relatively coarse resolution at the walls together with the hybrid URANS-LES method. The LES model, on the other hand, needs a much finer mesh also at the walls. The hybrid URANS-LES method are capable of capturing the flow field accurately even with the coarse resolution.

2.2 Paper B

Paper B is assigned to assess the ability of the scale-adaptive simulation (SAS) method to capture the vortex breakdown in highly swirling flows. The strongly swirling turbulent flow through an abrupt expansion is investigated using LES and SAS, to shed more light on the stagnation region and the helical precessing vortex. It is known that the large-scale helical vortex can be captured by the conventional URANS models. However, the spurious suppression of the small-scale structures should be avoided using less diffusive methods. The dynamics of the flow is studied at two Reynolds numbers, $Re = 6.0 \times 10^4$ and $Re = 10^5$, at an almost constant high swirl number of $Sr \sim 1.2$. The time-averaged velocity field and the root mean square of the velocity fluctuations are validated and investigated quantitatively. The flow with the lower Reynolds number gives a weaker outburst, while the frequency of the structures seems to be constant for a constant high swirl number. Both models are capable of capturing the physics of the flow, while SAS predicts turbulent structures better than LES immediately after the expansion using a relatively coarse mesh. The case with $Re = 6.0 \times 10^4$ has larger flow structures, for which LES presents a better agreement with the experimental results compared with the other operation condition, $Re = 10^5$. The SAS model has an extra term in the "ω" equation which is responsible for detecting the unsteadiness. The SAS term switches itself on and increases "ω". This leads to resolve the turbulent structures especially in the region after the expansion. The SAS method predicts the highly swirling flows at moderately high Reynolds numbers better than LES using a relatively coarse resolution.

2.3 Paper C

Paper C delineates the physics of the highly swirling turbulent flow through a suddenly expanding circular pipe, using a wide range of operating conditions and advanced turbulence treatments. The delayed DES Spalart-Allmaras (DDES-SA), improved DDES-SA (IDDES-SA), a dynamic k-equation LES (oneEqLES), dynamic Smagorinsky LES (dynSmagLES) and implicit LES with van Leer discretization (vanLeerILES) are scrutinized. A comprehensive mesh study is carried out and the results are validated with experimental data. The LES and DES results of different operating conditions are compared and described qualitatively and quantitatively. The features of the flows are distinguished mainly owing to different level of the centrifugal force for different swirls. The numerical results capture the vortex breakdown with its characteristic helical core, the Taylor-Görtler and the turbulence structures. The hybrid behavior of DDES-SA and IDDES-SA is discussed. The results confirm that LES and DES are capable of capturing the turbulence intensity, the turbulence production. and the anisotropy of the flow fields. The DDES-SA model is capable of capturing the physics of the flow with reasonable accuracy while still being sensitive to the wall-parallel resolution. The IDDES-SA behaves as a wall-modeled LES in the flows with high recirculation level although, no turbulent content is applied at the inlet. The distribution of the on-axis recirculation region varies with different Re and Sr. The intertwined nature of the coherent structure due to the vortex breakdown is wider and steeper for higher Re and Sr.

The dominant frequency of the flow, due to the precessing helical vortex, is insensitive to Re and Sr about unity. The level of the turbulence and the turbulence production increases remarkably with the swirl number, while the state of isotropy is not susceptible to Re and Sr. The flow is anisotropic immediately after expansion, while it further downstream rapidly becomes isotropic due to the redistribution between velocity fluctuations.

2.4 Paper D

Paper D presents a series of numerical simulation to study a highly swirling turbulent flow generated by the rotor-stator interaction. Four high-Reynolds number URANS, two low-Reynolds number URANS, three hybrid URANS-LES, and one LES turbulence models are scrutinized. These are standard $k-\epsilon$, SST $k-\omega$, realizable $k-\epsilon$ and RNG $k-\epsilon$, Launder-Sharma $k-\epsilon$ and Lien-Cubic $k-\epsilon$, three hybrid URANS-LES, delayed DES Spalart-Allmaras (DDES-SA), DDES SST $k-\omega$ (DDES-SST) and improved DDES-SA (IDDES-SA). The purpose is to understand effect of turbulence models in a swirling flow with a high level of unsteadiness, large pressure pulsations, and a significant level of generation and dissipation of turbulence in the main stream. In addition, a mesh resolution study is performed and the effects of boundary conditions on the flow are analyzed. The URANS models are capable of capturing the main feature of this flow, the vortex rope, which is formed by the strong centrifugal force. The force forms an on-axis recirculation region, which its size is overestimated by the URANS models. Although the low-Reynolds formulations treat the wall-effect in inter-blade passages more accurately, they still encounter difficulty to predict the size of the recirculation region. The anisotropy study of the flow shows that the conventional URANS models are inappropriate for such a swirling flow. The runner rotational fluctuation is a source of error which is absent in the numerical simulations. The turbulent structures in the runner affects the separation from the runner blade. These coherent and turbulent structures determine the character of the vortex rope and its disintegration. The hybrid method predicts these aspect of the flow reasonably well. The mesh generation is a vital part of the solution because the cells quality influences the flow circumstances qualitatively and quantitatively.

2.5 Paper E

Paper E presents the results of a rotation/curvature correction term, which is implemented with the shear stress transport model. The effects of curvature on turbulence quantities and the performance of added functionality of the SST $k-\omega$ with curvature corrector (SST-CC) model are explored. Turbulence-resolving simulations predict the flows in a swirl generator, resembling a Francis turbine working at 70% of the design point, and the Francis-99 working at the best efficiency point. Different quantities are compared with the results of the RNG $k-\epsilon$ and SST $k-\omega$ models. The RNG $k-\epsilon$, SST $k-\omega$ and SST-CC models are applied using wall functions with $30 < y^+ < 200$. The flows contain different levels of swirl and pressure pulsations. The results show that the SST-CC model presents a major improvement in predicting the on-axis recirculation region in the swirl generator. The SST-CC results are very similar to those of the other models for Francis-99. The SST-CC model predicts turbulence quantities very well in the middle of the on-axis recirculation region in the swirl generator but not at the entrance of the draft tube. It means that the multiplier f_{r1} does not act very well at the annular section of the draft tube where the swirl is quite strong. The model is tuned by manipulating the c_{r3} constant by $\pm 20\%$ in the production multiplier of f_{r1}. Some questions about f_{r1} still remain since the model does not capture unsteadiness in the upstream region of the draft tube. The study shows that the tuning of the model does not improve the quality of the results.

2.6 Paper F

Paper F provides a survey of the behavior of the vortex in a diffuser downstream a swirl generator, and assesses the ability of the URANS and hybrid URANS-LES models to predict the flow features. The flow unsteadiness generated in a swirl apparatus is investigated experimentally and numerically. The swirl apparatus has two parts: a swirl generator and a test section. The swirl generator which includes two blade rows, one stationary and one rotating, is designed such that the emanating flow at free runner rotational speed resembles that of a Francis hydro turbine operated at partial discharge. The test section consists of a conical diffuser similar to the draft tube cone of a Francis turbine. Several swirling flow regimes are produced and the LDA measurements are performed along three survey axes in the test section for different runner rotational speeds, [400rpm-920rpm], with a constant flow rate, 30 l/s. The experimental results show that the largest on-axis recirculation region, the largest precessing vortex rope, and the highest level of velocity fluctuations occur at the lowest rotational speed and the precessing vortex rope counter-rotates the runner. The experimental results of 600rpm operating condition show the lowest level of velocity fluctuations and a swirl that counter-rotates the runner in the on-axis stagnant region and co-rotates the runner in the outer region. The flow at 920rpm presents the narrowest on-axis recirculation region with a high level of velocity fluctuations in the draft tube. There is a strong vortex breakdown and a plunging motion of the vortex rope. The rotor-stator interaction is included when numerically reproducing the physics of the helical vortex in the draft tube. The results show that the rotor-stator interaction is necessary to capture the complexity of the flow structures. It is shown that the shape of the blade plays a more important role at 400rpm. The measured mean velocity components and its fluctuating parts are used to validate the results of unsteady numerical simulations, conducted using the FOAM-extend-3.0 CFD code. The RNG $k-\epsilon$ model reasonably predicts the main flow features in the draft tube at 600rpm, while the model overpredicts the on-axis recirculation region at the other rotational speeds. Since the linear eddy-viscosity models link the turbulent stress tensor and the mean strain rate they fail to model flows with a moderate or high level of swirl. The switching between URANS and LES modes in the DDES method suited well for internal flows with large vortical structures. The DDES-SA model presents realistic results also for 920rpm. The DDES-SA model predicts the resolved velocity fluctuations qualitatively correct downstream the runner. The total velocity fluctuations are in good agreement with experimental results. The numerical studies show that the wakes of the blades lose their coherence much faster at 400rpm than 920rpm. The predicted turbulent quantities are qualitatively and quantitatively correct at the throat. The DDES-SA model slightly underestimates the frequency of the precessing vortex rope at 400rpm and 920rpm.

2.7 Paper G

Paper G plausibly investigates the U9 Kaplan turbine model at two operating conditions using the conventional and non-conventional URANS models and a hybrid URANS-LES method. All clearances are included in the computational domain, such as the guide vane clearances, the runner blade tip-clearances, and the runner blade hub-clearances at both the leading and trailing edges. High-quality block-structured meshes are used to simulate the flow at the best efficiency point (BEP) and part load (PL) conditions with $Re = 1.6{\times}10^6$ and $Sr = 0.25$, and $Re = 1.39{\times}10^6$ and $Sr = 0.6$, respectively. The swirl number, Sr, is moderately low at BEP so that no vortex breakdown occurs, while it is high enough at PL to create a helical precessing *vortex rope* due to the vortex breakdown. The RNG $k-\epsilon$ model is employed as a conventional eddy-viscosity model. The explicit algebraic Reynolds stress model coupled with the SST $k{-}\omega$ model (EARSM) and the SST $k{-}\omega$ model with curvature correction modeling (SSTCC) are implemented and evaluated, as non-conventional URANS models. They are relatively easy to implement, economically tenable, and include more physics than the conventional turbulence models. The delayed detached eddy simulation method, coupled with the Spalart-Allmaras turbulence model (DDES-SA) is applied to gain a deep insight of the details of the flows. The DDES-SA simulations resolve the turbulent structures in the free-stream, but are three orders of magnitude more expensive than its URANS counterparts. The mean velocity components and their fluctuating parts are validated using experimental data. The URANS models are consistent with respect to the mean velocity at BEP, while only the non-conventional URANS models predict the mean velocity well at PL. At BEP, all turbulence models capture the structures in the flow field, such as the tip vortex, the hub vortices, the wakes of the blades and the on-axis structure. The hub jet affects the flow remarkably at this condition. The numerical results predict the jet and the tip-leakage flow very well. The RNG $k-\epsilon$ model particularly fails to capture the velocity fluctuations at BEP, while the non-conventional URANS models resolve the fluctuations remarkably well. The DDES-SA model predicts the mean velocity very well both at BEP and PL. The model accurately resolves the velocity fluctuations at BEP, while they are slightly underpredicted at PL. The non-conventional eddy-viscosity models EARSM and SSTCC slightly overpredict the recirculation region and capture a well resolved vortex rope. The RNG $k-\epsilon$ model captures the vortex rope, but predicts a four times wider recirculation region. The URANS models treat the boundary layers using the log-law wall-function, therefore the mesh generation process is more convenient than that for DDES-SA. The flow at PL is not in equilibrium close to the wall, and therefore a wall-function which includes non-equilibrium condition will improve the quality of the URANS models results.

Hybrid URANS-LES of such flows is still too expensive for industry. The costs of the hybrid URANS-LES method make it hard to use and push the researchers to stick to URANS. Thus, the use and development of non-conventional URANS and wall-functions which captures more physics, are still needed.

2.8 Paper H

Paper H presents a control technique to prevent or mitigate the vortex breakdown in the draft tube. The vortex rope in a conical diffuser of a swirl generator is controlled using continuous slot jets with different momentum fluxes and angles injected from the runner crown. The swirl generator is designed so that the flows without flow control resemble those different operating conditions of a Francis turbine. The study is undertaken with numerical modeling using the hybrid URANS-LES method. The comprehensive studies of Javadi and Nilsson (*Flow Turbul. combust.*, 2015), and Javadi, Bosioc, Nilsson, Muntean and Susan-Resiga (*ASME J. Fluids Eng.*, 2016) are considered as the base flows, and the effectiveness of the flow control technique used in the present work is compared with the validated numerical results presented in those studies. The base flows at two runner rotational speeds, 400rpm and 920rpm, are considered. Seven jets are studied, with different momentum fluxes, angles and positions. It is shown that

- For 400rpm, C3 is the jet with (U_r^+, U_θ^+, U_a^+) = (0, 2.62, 1.31) at position 1 and it shrinks the vortex rope more than what C6 with (U_r^+, U_θ^+, U_a^+) = (0, 2.62, 1.31) and C7 with (U_r^+, U_θ^+, U_a^+) = (0, 2.62, 3.93) do at position 2.
- For 920rpm, C1 is the jet with (U_r^+, U_θ^+, U_a^+) = (0, -2.62, 1.31) and C2 is the jet with (U_r^+, U_θ^+, U_a^+) = (0, -2.62, 2.62) at position 1. They shrink the vortex rope more effectively than what C4 with (U_r^+, U_θ^+, U_a^+) = (0, -2.62, 1.31) and C5 with (U_r^+, U_θ^+, U_a^+) = (0, -2.62, 3.93) do at position 2, because the jet at position 2 deals with a stronger swirl than that the jet does at position 1.
- The jet at position 1 is more effective than that at position 2.
- The tangential jet component is more important than the axial jet component in terms of shrinking the vortex rope.

The jet C1 can be considered as the most effective case in shrinking the vortex rope, and thus decreasing the velocity fluctuations and pressure pulsation. The best case studied in the present work is the jet of C1 with the volume flow rate of less than 3% of the discharge of the swirl generator. Thus, the injection of a continuous circumferential slot jet in the opposite direction of the main swirl of the flow is remarkably effective in shrinking the vortex rope. The momentum flux, the jet angle, and the jet position are decisive factors in the effectiveness of the technique.

3 Conclusion

A wide range of turbulence-resolving simulations is undertaken to investigate the swirling flows. The conventional and non-conventional URANS models, the hybrid URANS-LES methods and LES are implemented and scrutinized in different geometries and operating conditions. The strongly swirling turbulent flows through an abrupt expansion are explored using the DDES, SAS and LES methods. The DDES method is appropriate to predict highly swirling flows, while the method is still sensitive to the wall-parallel resolutions in highly swirling flows. The model does not switch to the LES mode for a coarse wall-parallel resolution. The switching between URANS and LES modes in the DDES method suited well for internal flows with large vortical structures. The SAS method has an extra term in the ω equation, which is responsible for detecting the unsteadiness. The flow field after expansion is intertwined and unsteady. The SAS term switches itself on and increases the ω. This leads to decrease the turbulent viscosity especially in the region after expansion. The SAS method predicts the flow field better than LES using a relatively coarse mesh. The SAS method encounters difficulties to detect the unfixed separation line from the hub in flow fields with high level of swirl. The state of turbulence in highly swirling flows is two-component dominated close to walls, which is why the log-law wall-function fails to realistically model the flow. A better choice is to use a wall-function which includes the non-equilibrium effects to model the flow more realistically.

A swirl generator with two types of guide vanes is investigated in different operating conditions using the rotor-stator interaction. The linear eddy-viscosity models reasonably predict the main flow features of the flow at the best efficiency point condition in the draft tube when the Sr is moderately low. The models overpredict the size of the on-axis recirculation region when the Sr exceeds a certain level at high- and part-load conditions. The low-Reynolds number turbulence models are also studied and it is shown that the models overpredicts the size of the on-axis recirculation region. Since the linear eddy-viscosity models link the turbulent stress tensor and the mean strain rate they fail to model flows with a moderate or high level of swirl. The non-conventional eddy-viscosity models slightly overpredict the recirculation region and capture a well resolved vortex rope.

The experience gained with the investigation of the swirl generator is used to study the U9 Kaplan turbine model in different operating conditions. The conventional and non-conventional URANS models, and the DDES method are scrutinized using the rotor-stator interaction. The DDES method plausibly predicts the highly swirling flow in the U9 Kaplan turbine model, while the simulation is three orders of magnitude more expensive than its URANS counterparts.

Hybrid URANS-LES of such flows is still too expensive for industry. The costs of the hybrid URANS-LES method make it hard to use and push the researchers to stick to URANS. Thus, the use and development of non-conventional URANS and wall-functions which captures more physics, are still needed.

References

[1] A. Javadi and H. Nilsson. "LES and DES of swirling flow with rotor-stator interaction". *Progress in Hybrid RANS-LES Modelling*. Ed. by S. Girimaji. Vol. 130. Springer-Verlag, 2014, pp. 457–468.

[2] A. Javadi and H. Nilsson. "A comparative study of scale adaptive and large-eddy simulations of highly swirling turbulent flow through an abrupt expansion". *IOP Conf. Ser.: Earth Environ. Sci.* Vol. 22. 2. 022017. 2014.

[3] A. Javadi and H. Nilsson. LES and DES of strongly swirling turbulent flow through a suddenly expanding circular pipe. *Comput. Fluids* **107** (2015), pp. 301–313. DOI: 10.1016/j.compfluid.2014.11.014.

[4] A. Javadi and H. Nilsson. Time-accurate numerical simulations of swirling flow with rotor-stator interaction. *Flow Turbul. Combust.* **95** (2015), pp. 755–774. DOI: 10.1007/s10494-015-9632-2.

[5] A. Javadi, E. Krane, and H. Nilsson. "Exploration of rotation/curvature correction method in hydropower application". *Turbulence, Heat and Mass Transfer 8*. Bosnia and Herzegovina, Sarajevo, 2015.

[6] A. Javadi, A. Bosioc, H. Nilsson, S. Muntean, and R. Susan-Resiga. Experimental and numerical investigation of the precessing helical vortex in a conical diffuser, with rotor-stator interaction. *ASME J. Fluids Eng.* (2016). DOI: 10.1115/1.4033416.

[7] A. Javadi and H. Nilsson. Detailed numerical simulations of a Kaplan turbine with rotor-stator interaction using turbulence-resolving simulations (2016). submitted to a scientific journal.

[8] A. Javadi and H. Nilsson. Active flow control of the vortex rope in a swirl generator. *Will be Published in Eng. App. Comput. Fluid Dyn.* (2016).

[9] A. Javadi and H. Nilsson. "Unsteady numerical simulation of the flow in the U9 Kaplan turbine model". *IOP Conf. Ser.: Earth Environ. Sci.* Vol. 22. 2. 022001. 2014.

[10] A. Javadi, A. Bosioc, H. Nilsson, S. Muntean, and R. Susan-Resiga. "Velocity and pressure fluctuations induced by the precessing helical vortex in a conical diffuser". *IOP Conf. Ser.: Earth Environ. Sci.* Vol. 22. 3. 032009. 2014.

[11] A. Javadi and H. Nilsson. "Active flow control of vortex rope in a conical diffuser". *IAHR WG Meeting on Cavitation and Dynamic Problems in Hydraulic Machinery and Systems, Ljubljana*. 2015.

[12] A. Javadi and H. Nilsson. "Advanced numerical prediction of strongly swirling turbulent flows". *5th International Workshop on Cavitation and Dynamic Problems in Hydraulic Machinery, September 9-11, Lausanne, Switzerland*. Vol. 23. 2013.

[13] S. Leibovich. Vortex stability and breakdown: survey and extension. *AIAA J.* **22** (1984), pp. 1192–206.

[14] V. Shtern and F. Hussain. Collapse, symmetry, breaking, and hysteresis in swirling flow. *Annu. Rev. Fluid Mech.* **31** (1999), pp. 537–566.

[15] J. Borda. Memoire sur l'ecoulement des fluides par les orifices des vases. *Memoire de l'academie Royale des Siences* (1766).

[16] A. Gupta, D. Lilley, and N. Syred. Swirl flows. *Kent: Abacus Press, Tunbridge Wells* (1984).

[17] P. Wang, X. Bai, M. Wessman, and J. Klingmann. Large eddy simulation and experimental studies of a confined turbulent swirling flow. *Phys Fluids* **16** (2004). DOI: http://dx.doi.org/10.1063/1.1769420.

[18] B. Guo, T. Langrish, and D. Fletcher. CFD simulation of precession in sudden pipe expansion flows with low inlet swirl. *Appl. Math. Model* **26**.1 (2002), pp. 1–15.

[19] A. Zohir, A. Abdel-Aziz, and M. Habib. Heat transfer characteristics in a sudden expansion pipe equipped with swirl generators. *Intl. J. Heat Fluid Fl.* **32** (2011), pp. 352–361.

[20] M. Escudier. Confined vortices in flow machinery. *Annu. Rev. Fluid Mech.* **19** (1987), pp. 27–52.

[21] P. Dellenback, D. Metzger, and G. Neitzel. Measurements in turbulent swirling flow through an abrupt axisymmetric expansion. *AIAA J.* **26**.6 (1988), pp. 669–681.

[22] P. Clausen, S. Koh, and D. Wood. Measurements of a swirling turbulent boundary layer developing in a conical diffuser. *Exp. Therm. Fluid Sci.* **6** (1993), pp. 39–48.

[23] P. Dörfler, M. Sick, and A. Coutu. *Flow-induced pulsation and vibration in hydroelectric machinery*. Springer-Verlag London, 2013. DOI: 10.1007/978-1-4471-4252-2.

[24] M. Nishi, X. Wang, K. Yoshida, T. Takahashi, and T. Tsukamoto. " An experimental study on fins, their role in control of the draft tube surging". *Hydraulic Machinery and Cavitation*. Dordrecht, Netherlands, 1996, pp. 905–914.

[25] M. Kjeldsen, K. Olsen, T. Nielsen, and O. Dahlhaug. " Water injection for the mitigation of draft-tube pressure pulsations". *IAHR International Meeting of W.G. on Cavitation and Dynamic Problems in Hydraulic Machinery and Systems*. Barcelona, Spain, 2006.

[26] R. Susan-Resiga, S. Muntean, V. Hasmatuchi, I. Anton, and F. Avellan. Analysis and prevention of vortex breakdown in the simplified discharge cone of a Francis turbine. *ASME-T J. Fluids Eng.* **132** (2010). 051102-1.

[27] C. Tănasă, A. Bosioc, S. Muntean, and S.-R. R. Flow-feedback method for mitigating the vortex rope in decelerated swirling flows. *ASME-T J. Fluids Eng.* **135**.6 (2013), pp. 1–11.

[28] A. Javadi and W. A. El-Askary. Numerical prediction of turbulent flow structure generated by a synthetic cross-jet into a turbulent boundary layer. *Intl. J. Num. Meth. Fluids* **69**.7 (2012), pp. 1219–1236.

[29] A. Javadi. Numerical predictions of slot synthetic jets in quiescent surroundings. *Intl. J. Prog. Comput. Fluid Dyn.* **13**.2 (2013), pp. 65–83.

[30] F. R. Menter and Y. Egorov. The scale-adaptive simulation method for unsteady turbulent flow predictions. part 1: theory and model description. *Flow Turbul. Combust.* **85** (2010), pp. 113–138.

[31] S. Girimaji. Partially-averaged Navier-Stokes model for turbulence: a Reynolds-averaged Navier-Stokes to direct numerical simulation bridging method. *ASME J. Appl. Mech.* **73**.3 (2006), pp. 413–421.

[32] R. Schiestel and A. Dejoan. Towards a new partially integrated transport model for coarse grid and unsteady turbulent flow simulations. *Theor. Comput. Fluid Dyn.* **18**.6 (2005), pp. 443–468.

[33] P. Spalart, W. Jou, M. Strelets, and S. Allmaras. " Comments on the feasibility of LES for wings and on a hybrid RANS-LES approach". *Comments on the feasibility of LES for wings and on a hybrid RANS-LES approach. Advances in DNS-LES, 1st AFOSR Int. Conf. on DNS-LES*. Columbus, OH: Greyden press, 1997.

[34] A. Javadi, A. Bosioc, H. Nilsson, S. Muntean, and R. Susan-Resiga. *Swirling flow in a conical diffuser generated with rotor-stator interaction*. Ed. by W. Rodi. 2016. URL: `http://qnet-ercoftac.cfms.org.uk/w/index.php/Main_Page`.

Appendix

A Implementation of two turbulence models

A.1 Elliptic-blending Reynolds Stress Model (EBRSM)

A.1.1 Introduction

Modeling the effects of solid walls on adjacent turbulent flows has long been—and still is—a major challenge. The problem is equally acute in one-point and two-point statistical closures, as it is in spectral modeling or large-eddy simulations (LES). Indeed, the hypotheses underlying existing one-point turbulence closure models, e.g., high Reynolds number, local isotropy, quasi-homogeneity, are not valid in the presence of a wall. Hence, near-wall modifications are necessary in order to make them comply with the near-wall behavior of turbulence.

In this contribution, Elliptic Blending Reynolds stress model (EBRSM) proposed by Manceau and Hanjalić [7] is implemented and verified in various flow fields. To blend the consistency and accuracy for industrial applications and simplicity of the model, EBRSM follows the elliptic blending model of Durbin [1]. Durbin's model enables the integration down to the wall, with acceptable grid density. The method, applied to Reynolds stress models, has a solid theoretical basis, but implies six additional equations, which impedes its spreading into the industry. The main problem is not the increased cost due to the number of equations, but rather the complexity of the implementation and the stability problems: the boundary conditions for the additional equations are a major source of numerical instability. The EBRSM reduces the number of equations in Durbin's Reynolds stress model and thus to reduce the complexity of the model.

A.1.1.1 The Physics of Wall Effects on Turbulence

A solid wall exerts multiple effects on fluid flow and turbulence. There are two fundamental mechanisms by which a solid boundary affects turbulence : (i) generation of a mean velocity gradient (via the no-slip condition) which, upon interaction with turbulent shear stress, supplies energy to turbulence ; and (ii) suppression (or blocking) of velocity fluctuations in its vicinity. The first effect can be regarded as dynamical and the second effect may be viewed as primarily kinematic. Here, it is hypothesized that the two effects are separate in affecting flow dynamics.

There is evidence that both the hairpins and streaks may be due to the effect of shear rate rather than due to the suppression of turbulence by the wall. For example, Uzkan and Reynolds [2] conducted a shear-free turbulent boundary-layer experiment by passing grid-generated turbulence over a moving wall. When the speed of the moving wall was matched to that of the free stream, a shear-free boundary layer was produced and the near-wall streaks disappeared in the absence of mean shear. A related experiment was performed by Thomas and Hancock [3] at a higher Reynolds number. Rogers and Moin [4], using direct numerical simulation of a homogeneous shear flow, found the presence of hairpin vortices similar to those observed in the logarithmic layer of wall-bounded turbulent flows. However, their computed velocity patterns did not reveal elongated streaky structures; in fact, the shear rate in their computation was comparable with that in the logarithmic layer of a turbulent boundary layer. It should be noted that in a homogeneous turbulent flow there is no solid boundary to suppress velocity fluctuations.

The effect of blocking velocity fluctuations near a surface leads to a net transfer of energy from the vertical component of turbulence to the horizontal components [5]. This redistribution effect appears to be the reason why the vertical component of the pressure-strain-rate term, $\overline{p\partial v/\partial y}$, changes sign in the vicinity of the surface [6]. However, the effect of the boundary is not important for small eddies at $y \geq L$, where L is the integral length scale. A physically consistent model ought to account separately for each of the effects mentioned, something that is difficult to achieve with a limited number of flow and turbulence parameters that are at one's disposal in one-point turbulence models, regardless of their level. Thus, the behavior of the flow should be taken into account in correct modelling of the wall effects.

Most models of near-wall turbulence do not distinguish the viscous from nonviscous effects and usually apply empirical damping functions in terms of local turbulence Reynolds numbers and often of wall distance by which to account for the total wall effect. Needless to say, such models cannot perform well in situations where one or the other effect is absent or is of less importance (e.g., viscous and transitional regions in flows away from a solid wall unaffected by blocking, or flows with liquid–gas interface where the kinematic blocking is the sole cause of turbulence modification). A better approach should considered to account for both effects.

A.1.1.2 Rationale of Elliptic Blending Model

The elliptic blending model reduces the number of equations in Durbin's Reynolds stress model and thus the complexity of the model. Durbin's model with six elliptic differential equations with boundary conditions enables the reproduction of the near-wall behavior of the redistribution term. These equations have then the purely geometrical effect, with a unique length scale, L. Their role is to enforce the redistribution terms to comply with their near-wall limiting behavior. It is, therefore, expected that the same effect could be reproduced with only one elliptic equation, $\alpha - \nabla^2\alpha = 1/k$, where α is elliptic function and k is the turbulent kinetic energy.

The Reynolds stresses behave as y^2 , if y represents the direction normal to a wall located in y=0 (the behaviour in y^n , with $n > 2$, is due to the blockage effect). The boundary condition $u_i u_j = 0$ is not sufficient to impose this behaviour, which requires the correct reproduction of the balance between viscous diffusion and dissipation in the Reynolds stress transport equations in the vicinity of the wall. This requirement is consequently linked to the correct modelling of the dissipation tensor: since the viscous damping also suppresses the scale separation between energetic and dissipative structures, the anisotropy of the dissipation tensor cannot be neglected. In practice, the correct asymptotic behaviour is obtained in near-wall Reynolds-stress models by choosing a model for the dissipation tensor that satisfies

$$\lim_{y\to 0} \epsilon_{ij} = 2\nu \lim_{y\to 0} \frac{\overline{u_i u_j}}{y2}. \tag{1}$$

The implementation of the boundary condition for ϵ in the OpenFOAM-2.3x code is

```
forAll(mesh_.boundary(),i)}
{
if(mesh_.boundary()[i].type()=="wall")
    {
```

```
    scalarField & refepsilonboundary = epsilon_.boundaryField()[i];
    scalarField knearwall  = k_.boundaryField()[i].patchInternalField();

        epsilon_.boundaryField()[i].patchInternalField()=
            2.0/nearWallDist(mesh_).y()[i]/nearWallDist(mesh_).y()[i]
            *nu()*mag(knearwall);
    }
}.
```

For a free-slip surface, components $\overline{u^2}$ and $\overline{w^2}$ behave as y^0 and $\overline{v^2}$ as y^2; for a no-slip surface, this asymptotic behaviour is changed to y^2 and y^4, respectively. In all cases, the most important effect to take into account is the fact that $\overline{v^2}$ is negligible compared to the other normal stresses, such that turbulence reaches a *two-component* limit in the vicinity of the surface. In the case of a no-slip wall, one of the main difficulties lies in the particular scales of this phenomenon, linked to the non-locality of the fluctuating pressure, at the origin of a sensitivity of turbulence to the blockage effect up to a distance to the wall much larger than the thickness of the viscous sublayer. In order to model this blockage effect, the correct reproduction of the near-wall balance between viscous diffusion and dissipation, Eq. 1, is not sufficient: the asymptotic behaviour of the velocity-pressure gradient correlation term must be accounted for. This is the main purpose of the Elliptic Blending method.

The presence of a wall induces an increase of pressure fluctuations, called the *wall-echo* effect. In RANS modelling, the wall echo effect specifically denotes the consequence of the existence of this echo for the velocity-pressure gradient correlation involved in the Reynolds stress transport equations. The wall blockage and the wall echo are always coupled. In terms of modelling, it is important to remark that the two effects have opposite influences on pressure-strain term in most of the near-wall region, in particular for its redistributive part.

The main objective of Elliptic Relaxation and Elliptic Blending approaches is to account for the influence of the wall blockage on the energy redistribution towards the wall-normal component, which is necessary to reproduce the two-component limit of turbulence.

A.1.2 The Elliptic Blending Approach

Equation 2 shows the pressure-strain term in the EBRSM,

$$\phi_{ij} = (1-\alpha^3)\phi_{ij}^w + \alpha^3 \phi_{ij}^h, \tag{2}$$

where ϕ_{ij}^h is a standard model of the rapid part in the pressure-strain term. The main feature of Elliptic Blending, the reproduction of the blockage effect, is due to the fact that the elliptic operator ensures a smooth relaxation from the correct asymptotic behaviour of ϕ_{ij}, pressure-strain term, imposed by the boundary conditions to the standard model ϕ_{ij}^h, see Eq. 2. Manceau and Hanjalić [7] proposed the Elliptic Blending approach, for the purpose of building a model preserving the desirable features of Elliptic relaxation.

The method consists in ensuring the transition from the near wall to the weakly inhomogeneous behaviour using a single scalar function, α in Eq. 2, which must tend to 0 at the wall and to 1 far from the wall. The near-wall form of the pressure-strain term is ϕ_{ij}^w. The function α reads

$$\alpha - L^2\nabla^2\alpha = 1. \tag{3}$$

The implementation in the code is

```
tmp<fvScalarMatrix> alphaEqn
    (
    fvm::Sp(OneoverL2,alpha_)
   -fvm::laplacian(One,alpha_)
        ==
        OneoverL2
    );
    alphaEqn().relax();
    solve(alphaEqn);
```

where `OneoverL2` is

```
volScalarField OneoverL2 =1./(L*L);
```

with the boundary condition $\alpha = 0$ at the wall. The solution of this equation goes to zero at the wall and to one far from the wall, thus providing the appropriate blending between the two formulations ϕ_{ij}^h and ϕ_{ij}^w. The thickness of the region of influence of the near-wall model is driven by the length scale L,

$$L = C_L max\left(\frac{k^{3/2}}{\epsilon}, C_\eta \frac{\nu^{3/4}}{\epsilon^{1/4}}\right), \tag{4}$$

which is implemented in the code as

```
volScalarField L = CL * max(pow(k_,1.5)/epsilon_,
                   Ceta * pow(nu(), 0.75)/pow(epsilon_,0.25));
```

where C_L and C_η are constant.

The term ϕ_{ij}^h in Eq. 2 reads

$$\begin{aligned}\phi_{ij}^h = -\left(g_1 + g_1^*\frac{P}{\epsilon}\right)\epsilon a_{ij} + g_2\epsilon\left(a_{ik}a_{kj} - \frac{1}{3}a_{kl}a_{kl}\delta_{ij}\right) \\ + \left(g_3 - g_3^*\sqrt{a_{kl}a_{kl}}\right)kS_{ij} \\ + g_4 k\left(a_{ik}S_{jk} + a_{jk}S_{ik} - \frac{2}{3}a_{lm}S_{lm}\delta_{ij}\right) \\ + g_5 k\left(a_{ik}W_{jk} + a_{jk}W_{ik}\right),\end{aligned} \tag{5}$$

where $a_{ij} = \overline{u_i u_j}/2k - \delta_{ij}/3$ is the anisotropy tensor, S_{ij} is the strain rate tensor and W_{ij} is the vorticity tensor, P is the the trace of production tensor.

Note that in this version of the model $g_2 = 0$. Now, the model is not very sensitive to a coarsening of the near-wall mesh, as long as the first point is located in the viscous sublayer ($y^+ < 5$). To introduce ϕ_{ij}^h, the strain and vorticity rates are needed. They are implemented as

```
volTensorField    gradU =  fvc::grad(U_);
volTensorField    S = 0.5*((gradU.T()+gradU));
volSymmTensorField Ssym = symm(S);
volTensorField    W = 0.5*((gradU.T()-gradU));
```

where S and W are strain and vorticity, respectively. The anisotropy and pressure-strain terms are implemented as

```
volSymmTensorField a = dev(R_)/tr(R_);

volSymmTensorField isotrope =
        1.0/3.0*alpha_*alpha_*alpha_*(g1*epsilon_ + g1star*G)*I;

volScalarField anisotrope =
        alpha_*alpha_*alpha_*(g1*epsilon_ + g1star*G)/2.0/k_;

volSymmTensorField phih =
        k_*symm(S*(g3-g3star*sqrt(a&&a)))
        +g4*k_*(twoSymm(a & S) - 2.0/3.0*I* (a && S) )
        +g5*k_*twoSymm(a & W.T());
```

where `isotrope` and `anisotrope` are the diagonal and deviatoric parts of first term in ϕ^h_{ij}, respectively.

The term ϕ^w_{ij} in Eq. 2 reads

$$\phi^w_{ij} = -5\frac{\epsilon}{k}\left(\overline{u_i u_k}n_j n_k + \overline{u_j u_k}n_i n_k - \frac{1}{2}\overline{u_i u_k}n_k n_l n_j n_j - \frac{1}{2}\overline{u_k u_l}n_k n_l \delta_{ij}\right), \tag{6}$$

where n is wall normal vector which reads

$$n = \frac{\nabla\alpha}{\|\nabla\alpha\|}, \tag{7}$$

where the implementation of $\nabla\alpha$ and n is

```
volVectorField gradalpha = fvc::grad(alpha_);
volVectorField n = gradalpha/mag(gradalpha);
```

where n is used to implement other terms of the pressure-strain term.

Different terms of ϕ^w_{ij} and ϕ_{ij} are implemented as

```
volVectorField Rn = R_&n;
volTensorField Rnn = Rn*n;

 volSymmTensorField phiw = -5.0*epsilon_/k_*
    symm(
    (Rnn + Rnn.T() -0.5*((R_ & n & n)* (n*n + I)))
    );

volSymmTensorField phi =
       (One - alpha_*alpha_*alpha_)* phiw
       + alpha_*alpha_*alpha_*phih;
```

where `phi` corresponds with ϕ (the pressure-strain term).

A.1.3 Elliptic Blending Reynolds-stress Model

The Reynolds-stress transport equation reads

$$\frac{D\overline{u_i u_j}}{Dt} = P_{ij} + D^{\nu}_{ij} + D^{T}_{ij} + \phi_{ij} - \epsilon_{ij}, \tag{8}$$

where P_{ij}, D^{ν}_{ij}, D^{T}_{ij}, ϕ_{ij} and ϵ_{ij} stands for the production, the molecular diffusion, the turbulent diffusion, the pressure-strain correlation and the dissipation tensor, respectively. The implementation of the pressure-strain term is discussed in section 2. The implementation of the other terms are discussed in this section. The turbulent diffusion is given by

$$D^{T}_{ij} = \frac{\partial}{\partial x_l}\left(\frac{C_\mu}{\sigma_k}\overline{u_l u_m} T \frac{\partial \overline{u_i u_j}}{\partial x_m}\right). \tag{9}$$

This term is implemented in the Reynolds-stresses equation at the end of this section. The dissipation tensor is given by

$$\epsilon_{ij} = \left(1-\alpha^3\right)\frac{\overline{u_i u_j}}{k}\epsilon + \frac{2}{3}\alpha^3 \epsilon \delta_{ij}. \tag{10}$$

The implementation of the dissipation tensor is done as

```
volScalarField epsilonterm1 =
       (One- alpha_*alpha_*alpha_)*epsilon_/k_;
volSymmTensorField epsilonterm2 =
       2.0/3.0 * I* alpha_*alpha_*alpha_*epsilon_
       + 0.0*((One- alpha_*alpha_*alpha_)*epsilon_/k_)*R_;
```

where, `One` is a scalar 1 and `epsilon_` is calculated from the dissipation equation in the following.
Time scale is given by

$$T = max\left(\frac{k}{\epsilon}, C_T\left(\frac{\nu}{\epsilon}\right)^{1/2}\right), \tag{11}$$

which is implemented as

```
volScalarField TEBM = max(k_/epsilon_, CT * sqrt(nu()/epsilon_));
```

where C_T is constant. The time scale is used both in dissipation and Reynolds stress equations.

The dissipation equation is given by

$$\frac{D\epsilon}{Dt} = \frac{C'_{\epsilon 1}P - C_{\epsilon 2}\epsilon}{T} + \frac{\partial}{\partial x_l}\left(\frac{C_\mu}{\sigma_\epsilon}\overline{u_l u_m} T \frac{\partial \epsilon}{\partial x_m}\right) + \nu\frac{\partial^2 \epsilon}{\partial x_k \partial x_k} \tag{12}$$

$$C'_{\epsilon 1} = C_{\epsilon 1}\left[1 + A_1(1-\alpha^3)\frac{P}{\epsilon}\right] \tag{13}$$

where, $C'_{\epsilon 1}$ given by Eq. 13 is implemented as

```
volScalarField Cepsilon1bar =
            Cepsilon1* (1.0 + A1*(One-alpha_*alpha_*alpha_)
            *(G/epsilon_));.
```

The dissipation equation, Eq. 12, is implemented as

```
tmp<fvScalarMatrix> epsEqn
(
    fvm::ddt(epsilon_)
  + fvm::div(phi_, epsilon_)
  - fvm::Sp(fvc::div(phi_), epsilon_)
  - fvm::laplacian(CMu/sigmaepsilon*R_*TEBM, epsilon_)
  - fvm::laplacian(nu(), epsilon_)
    ==
  - fvm::Sp(Cepsilon2/TEBM, epsilon_)
  + Cepsilon1bar*G/TEBM
);
epsEqn().relax();
solve(epsEqn);
```

where the two laplacian terms on the right-hand side are turbulent and viscous diffusion, respectively.

The implementation of the Reynolds-stress equation, Eq. 8, is done as

```
tmp<fvSymmTensorMatrix> REqn
(
    fvm::ddt(R_)
    + fvm::div(phi_, R_)
    - fvm::Sp(fvc::div(phi_), R_)
    - fvm::laplacian(nu(), R_)
    - fvm::laplacian(CMu/sigmak*TEBM*R_,R_)
    + fvm::Sp(anisotrope, R_)
    + fvm::Sp(epsilonterm1, R_)

  ==

    P
    + isotrope
    - epsilonterm2
    + phistar
);
REqn().relax();
solve(REqn);
```

where terms on the right-hand side of the equation is introduced implicitly.

The coefficients are given by
$g_1 = 3.4$, $g_1^* = 1.8$, $g_3 = 0.8$, $g_3^* = 1.3$, $g_4 = 1.25$, $g_5 = 0.4$, $C_\mu = 0.21$, $\sigma_k = 1.0$, $C_T = 6.0$, $C_L = 0.133$, $C_\eta = 80.0$, $C_\epsilon 1 = 1.44$, $C_\epsilon 2 = 1.83$, $A_1 = 0.065$, $\sigma_\epsilon = 1.15$.

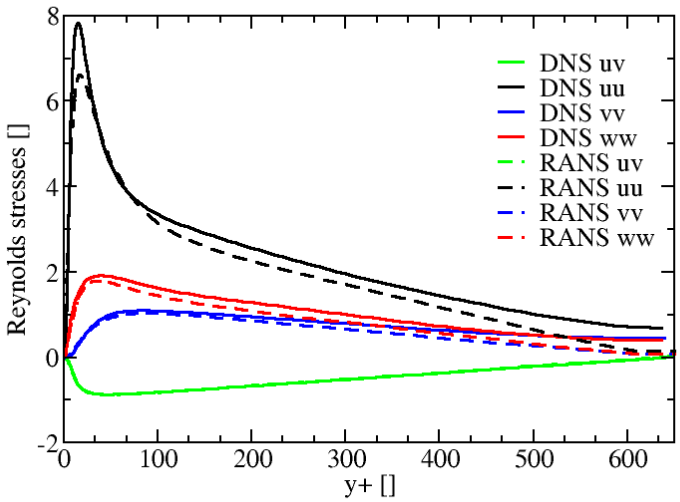

Figure 1: Reynolds stresses in the channel, $Re_\tau = 590$.

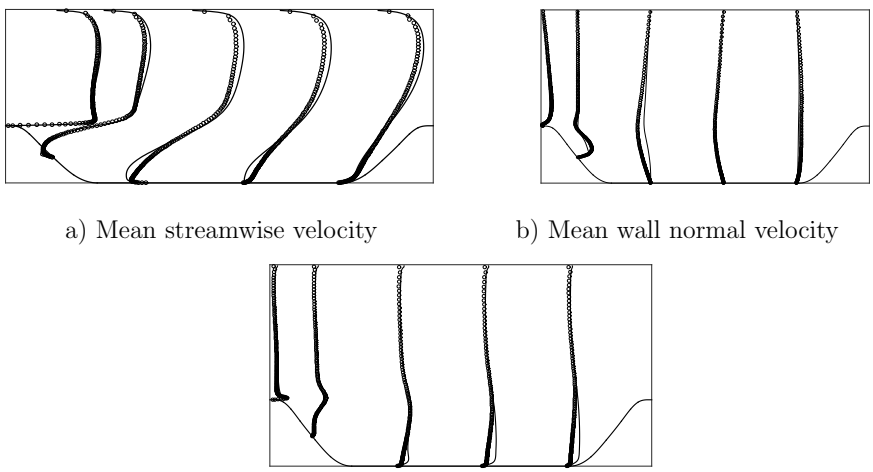

a) Mean streamwise velocity

b) Mean wall normal velocity

c) Mean streamwise velocity fluctuation

Figure 2: a) streamwise mean velocity b) wall normal mean velocity c) streamwise Reynolds stress over the periodic hill, marker: experiments, solid line: EBRSM.

A.1.4 Validation of the Implementation

The implementation is validated with four test cases

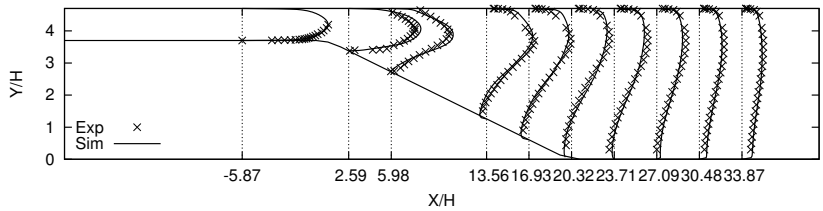

a) Mean streamwise velocity

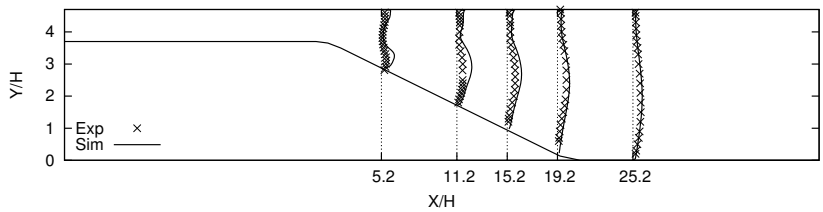

b) Mean streamwise velocity fluctuation

Figure 3: a) streamwise mean velocity b) Reynolds stresses in the asymmetric diffuser

- channel flow with $Re_\tau = 590$
- periodic hill with $Re = 10595$
- a symmetric diffuser with $Re = 18000$
- Dellenback abrupt expansion with $Re = 100000$, $Sr = 1.23$.

The calculations reported herein are made using the finite-volume method in the OpenFOAM-2.3x CFD code. The second-order central differencing scheme is used to discretize the diffusion terms. The linear-upwind differencing is used to approximate the convection term. Time marching is performed with an implicit second-order accurate backward differentiation scheme. The solver used in all simulations is *pisoFoam*.

A.1.4.1 Channel Flow

The Reynolds number based on the wall stress is $Re_\tau = 595$. Periodic boundary conditions are applied in the streamwise direction. The mesh is $N_x \times N_y = 80 \times 5$. The pressure gradient that drives the flow is adjusted dynamically to maintain a constant mass flux through the channel. The results are compared with the DNS of Moser et al. [9], see Fig. 1.

A.1.4.2 Periodic Hill

The Reynolds number, $Re = 10595$ is based on the hill height h, the bulk velocity taken at the crest of the first hill, and the laminar viscosity. The domain dimensions are $9.0h \times 3.036h$, $h = 28mm$ and the flow is periodic in the streamwise direction. The mesh is $N_x \times N_y = 87 \times 85$. The cyclic boundary condition with constant bulk velocity is applied at the inlet. The results are compared with the LES results of Frohlich et al. [8], see Fig. 2.

A.1.4.3 Asymmetric Diffuser

The configuration is an asymmetric plane diffuser, see Fig. 3, with a Reynolds number of $Re = U_{b,in}H/\nu = 18000$ ($H_{in} = 1$). The diffuser angle is 10°. The mesh is $N_x \times N_y = 2070 \times 80$. The homogeneous Neumann is applied for the turbulence quantities at the outlet boundary. The *inletOutlet* condition, which is the homogeneous Neumann condition with a limitation of no backflow, is applied at the outlet boundary for the velocity. The homogeneous Neumann condition is applied for the pressure at all boundaries. The results are compared with the experimental study of Buice and Eaton [10], see Fig. 3.

A.1.4.4 Dellenback Abrupt Expansion

The case studied in the present work is the swirling flow through a sudden 1:2 axisymmetric expansion that was experimentally examined by Dellenback et al. [12]. The origin is located on the centerline at the expansion. The inlet Reynolds number is 10^5, and the swirl number is 1.23. For more details about flow configuration and boundary conditions see Javadi and Nilsson ref. [11]. The mesh consists of 1.8×10^6 cells with 4.5×10^5 cells in the upstream of the expansion. Figure 4 shows the mean velocity and velocity fluctuation root mean square at $z/D = 0.25$. The EBRSM results show good agreement with experimental results. The main character of the flow, the vortex breakdown, is captured very well.

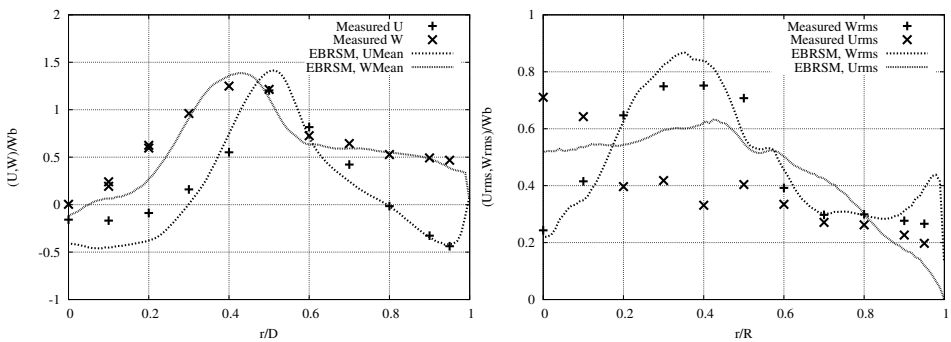

Figure 4: a) axial, W, and tangential, U, mean velocity normalized by bulk velocity at $z/D = 0.25$, b) axial, $Wrms$, and tangential, $Urms$, velocity fluctuation root mean square normalized by bulk velocity at the inlet,

A.2 The Partial Integrated Transport Model based on EBRSM

In this section the methodology of a seamless hybrid URANS-LES and its extensions into the EBRSM is discussed. The readers are referred to follow original articles for a detailed presentation of all the steps of the derivation of this approach [13, 14].

The EBRSM is adapted with the hybrid URANS-LES approach using the partial integrated transport model (PITM) methodology. In the PITM approach initially proposed by Schiestel and Dejoan [13], the amount of resolved energy is to be controlled by making the equations of the model dependent on the filter width. This can be achieved by using a transport equation for the dissipation rate that is a modification of the usual equation used in URANS. In order to reproduce the complex production and redistribution when the cutoff wavenumber, κ_c, is located in the productive zone of the turbulent energy spectrum, the model is based on transport equations for the subgrid-stress tensor, see Fig. 5. The cutoff wavenumber, κ_c, and thus the transition from URANS to LES is controlled by making the $C_{\epsilon 2}$ coefficient in the dissipation equation of a URANS model a function of κ_c. As a result of modeling in spectral space, with a variable cutoff wavenumber κ_c, compatibility is guaranteed with URANS ($\kappa_c \rightarrow 0$) and LES. When the cutoff wavenumber goes to zero, such that all the turbulent scales are modeled. It is noteworthy that The total fluctuating kinetic energy is defined by $k = k_m + k_r$, which k_m is modeled part and k_r is the resolved part of the energy. Thus, the modifying of the destruction term in the dissipation equation occurs by introducing the value $C^*_{\epsilon 2}$,

$$C^*_{\epsilon 2} = C_{\epsilon 1} + r(C_{\epsilon 2} - C_{\epsilon 1}), \tag{14}$$

where $C_{\epsilon 1}$ and $C_{\epsilon 2}$ are constant and $r = k_m/k$ is the ratio modeled energy over total energy, which is dependent on the cutoff wavenumber. The parameter r controls the transition from a URANS to a LES behavior, the URANS equation being recovered when r=1. When r is reduced, typically around the value 0.2, the cutoff wavenumber is well in the inertial range of the energy spectrum. When the mesh is locally coarse compared to a LES mesh, the cutoff wavenumber can be located in the productive zone of the spectrum, where equilibrium is rarely achieved, and in such a case, determining the length scale

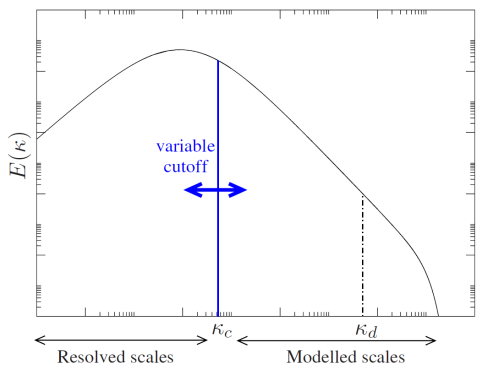

Figure 5: (Color online) Definition of the wavenumbers κ_c and κ_d [14].

through transport equations for dissipation and SGS energy (or SGS stresses) is crucial. Furthermore, in the inertial range of the spectrum, second-moment closures and eddy-viscosity models for the SGSs are equivalent, due to the equilibrium and the isotropy pertaining to these scales. When the model is neither in RANS mode nor in LES mode, i.e., when the cutoff wavenumber is in the productive region of the spectrum (VLES model), the situation is different. The SGSs are subject to large-scale strain variations, and in such a case, the eddy-viscosity models fail and, in particular, the phase lag between stress and strain must be accounted for.

The implementation of the PITM methodology based on EBRSM is limited to solve the transport equations a SGS and the new constants and the quantity $r = k_m/k$ should be considered as well. The pressure-strain term is

$$\phi_{ij_{SGS}} = (1-\alpha^3)\phi_{ij}^w + \alpha^3\phi_{ij}^h, \tag{15}$$

where

$$\phi_{ij}^w = -5\frac{\epsilon_{SGS}}{k_{SGS}}\left(\overline{u_iu_k}n_jn_k + \overline{u_ju_k}n_in_k - \frac{1}{2}\overline{u_iu_k}n_kn_ln_jn_j - \frac{1}{2}\overline{u_ku_l}n_kn_l\delta_{ij}\right), \tag{16}$$

and,

$$\begin{aligned}\phi_{ij}^h = -\left(g_1 + g_1^*\frac{P_{SGS}}{\epsilon_{SGS}}\right)\epsilon_{SGS}a_{ij} + g_2\epsilon_{SGS}\left(a_{ik}a_{kj} - \frac{1}{3}a_{kl}a_{kl}\delta_{ij}\right)\\ + \left(g_3 - g_3^*\sqrt{a_{kl}a_{kl}}\right)k_{SGS}S_{ij}\\ + g_4k_{SGS}\left(a_{ik}S_{jk} + a_{jk}S_{ik} - \frac{2}{3}a_{lm}S_{lm}\delta_{ij}\right)\\ + g_5k_{SGS}\left(a_{ik}W_{jk} + a_{jk}W_{ik}\right).\end{aligned} \tag{17}$$

The dissipation tensor is given by

$$\epsilon_{ij_{SGS}} = \left(1-\alpha^3\right)\frac{\overline{u_iu_j}}{k_{SGS}}\epsilon_{SGS} + \frac{2}{3}\alpha^3\epsilon_{SGS}\delta_{ij}. \tag{18}$$

The dissipation equation is given by

$$\frac{D\epsilon_{SGS}}{Dt} = \frac{C_{\epsilon1}'P_{SGS} - C_{\epsilon2}^*\epsilon_{SGS}}{T} + \frac{\partial}{\partial x_l}\left(\frac{C_\mu}{\sigma_{\epsilon_{SGS}}}\overline{u_lu_m}T\frac{\partial\epsilon_{SGS}}{\partial x_m}\right) + \nu\frac{\partial^2\epsilon_{SGS}}{\partial x_k\partial x_k} \tag{19}$$

where the time scale is

$$T = max\left(\frac{k_{SGS}}{\epsilon_{SGS}}, C_T\left(\frac{\nu}{\epsilon_{SGS}}\right)^{1/2}\right), \tag{20}$$

and,

$$C_{\epsilon1}' = C_{\epsilon1}\left[1 + A_1(1-\alpha^3)\sqrt{\frac{k_{SGS}}{\overline{u_iu_j}n_in_j}}\right]. \tag{21}$$

The main problem in PITM is the calculation of r, which is the ratio of modeled energy over total energy. Since the final value of the mean modeled, k_m and resolved,k_r, parts of kinetic energy are calculated when the simulation is finished, the value of $C_{\epsilon2}^*$, Eq. 14 is calculated using a dynamic approach with following steps:

- The energy ratio is monitored during the calculation by evaluating the resolved energy and the total energy. This ratio is called the observed ratio, r^o.
- This ratio is compared to the ratio used in which is called the target ratio, r^t, which reads

$$r^t = min\left[1;\ (1-\alpha^2)\ +\ \alpha^2\ \frac{1}{\beta_0 \eta_0^{2/3}}\right], \tag{22}$$

  which $\beta_0 = 0.2$ and $\eta = \frac{\pi}{\Delta}\frac{k^{3/2}}{\epsilon}$, Δ is the filter width.
- The coefficient $C^*_{\epsilon 2}$ entering the dissipation equation is replaced by $C^*_{\epsilon 2} + \delta C^*_{\epsilon 2}$ in order to drive the observed ratio toward the target ratio. The value $\delta C^*_{\epsilon 2}$ reads

$$\delta C^*_{\epsilon 2} = 2\ (C^*_{\epsilon 2} - 1)\left(\frac{r^t}{r^o}\right). \tag{23}$$

The implementation in the code is

```
volScalarField kr = 0.5*(UPrime2Mean_.component(tensor::XX)
                  + UPrime2Mean_.component(tensor::YY)
                  + UPrime2Mean_.component(tensor::ZZ));

const scalar    pi (M_PI);

volScalarField eta = pi*pow(kMean_,1.5)/delta()/epsilonMean_;

volScalarField r0 = kMean_/(kr+kMean_);

volScalarField rt = min(One, (One-alpha_*alpha_)
                  + alpha_*alpha_/beta0_/pow(eta, 0.667));

volScalarField Cepsilon2star =
        Cepsilon1_ + rt*(Cepsilon2_-Cepsilon1_);
volScalarField deltaCepsilon2star =
        2 * (Cepsilon2star-One)*(rt/r0-One);
Cepsilon2star = Cepsilon1_ + rt*(Cepsilon2_- Cepsilon1_)
               + deltaCepsilon2star;
```

References

[1] Durbin, P.A.: Near-wall turbulence closure modeling without 'damping functions'. Theor. Comput. Fluid Dyn. 3(1), (1991)

[2] Uzkan, T. and Reynolds, W.C.: A shear-free turbulent boundary layer. J . Fluid Mech. 28, 803-821 (1967)

[3] Thomas, N.H. and Hancock, P.E.: Grid turbulence near a moving wall. J . Fluid Mech. 82, 481-496 (1977)

[4] Rogers, M.M. and Moin, P.: The structure of the vorticity field in homogeneous turbulent flows. J . Fluid Mech. 176, 33-66 (1987)

[5] Hunt, J. C. R. and Graham, J. M. R.: Free-stream turbulence near plane boundaries. J . Fluid Mech. 84, 209-235 (1978)

[6] Moin, P. and Kim, J.: Numerical investigation of turbulent channel flow. J . Fluid Mech. 118, 341-377 (1982)

[7] Manceau, R. and Hanjalić , K.: Elliptic blending model: a new near-wall Reynolds stress turbulence closure. Phys. Fluids 14(2), 744–754 (2002)

[8] Frohlich, J., Mellen, C. P., Rodi, W., Temmerman, L., and Leschziner, M.A.: Highly resolved large-eddy simulation of separated flow in a channel with streamwise periodic constrictions. J. Fluid Mech. 526, 19-66 (2005)

[9] Moser, R.D., Kim, J. and Mansour, N.N.: Direct numerical simulation of turbulent channel flow up to Re= 590. Phys. Fluids, 11(4), 943-945 (1999)

[10] Buice, C.U. and Eaton, J.K.:Experimental Investigation of Flow Through an Asymmetric Plane Diffuser. J. Fluids Eng.122, 433-435 (2000)

[11] Javadi, A. and Nilsson, H.: LES and DES of strongly swirling turbulent flow through a suddenly expanding circular pipe. Comput. Fluids 107, 301-313 (2015)

[12] Dellenback, P.A., Metzger, D.E. and Neitzel, G.P.: Measurements in turbulent swirling flow through an abrupt axisymmetric expansion. AIAA J. 26(6), 669–81 (1988)

[13] Schiestel, R. and Dejoan, A.: Towards a new partially integrated transport model for coarse grid and unsteady turbulent flow simulations. Theor. Comput. Fluid Dyn. 18(6), 443-468 (2005)

[14] Fadai-Ghotbi, A., Christophe F., Manceau, R. and Borée, J.: A seamless hybrid RANS-LES model based on transport equations for the subgrid stresses and elliptic blending. Phys. Fluids, 22(5) (2010)

B Appended papers A–H